Field Experimental Study of Dynamic Smagorinsky Models in the Atmospheric Surface Layer

JAN KLEISSL AND MARC B. PARLANGE

Department of Geography and Environmental Engineering, and Center for Environmental and Applied Fluid Mechanics, The Johns Hopkins University, Baltimore, Maryland

CHARLES MENEVEAU

Department of Mechanical Engineering, and Center for Environmental and Applied Fluid Mechanics, The Johns Hopkins University, Baltimore, Maryland

(Manuscript received 14 October 2003, in final form 22 April 2004)

ABSTRACT

An analysis of dynamic Smagorinsky models is performed based on the Horizontal Array Turbulence Study (HATS) dataset. In the experiment, two vertically separated horizontal arrays of 14 three-dimensional sonic anemometers were placed in the atmospheric surface layer. Subgrid-scale (SGS) and resolved quantities are derived from 2D filtering at a filter scale Δ and differentiation of filtered velocity fields. In a previous study the Smagorinsky coefficient $c_s^{(\Delta)}$ was computed directly from these data and found to depend on atmospheric stability and height above the ground. The present study examines the scale-invariant dynamic model of Germano et al. and the scale-dependent dynamic model of Porté-Agel et al. and tests their accuracy in predicting $c_s^{(\Delta)}$ and its dependencies on stability and height above the ground. The Germano identity uses a test filter at $\alpha\Delta$ (in this study $\alpha = 1.75$ is used). The coefficient is derived from various data test-filtered at this scale assuming that the Smagorinsky coefficient is scale invariant. The results show that the scale-invariant dynamic model severely underpredicts the coefficient and its trends whenever Δ is similar to, or larger than, the large-scale limit of the inertial range (typically the smaller of the height above the ground z or the Obukhov length L). The scale-dependent dynamic model uses a second test filter at scale $\alpha^2\Delta$ to deduce dependence of $c_s^{(\Delta)}$ on the filtering scale. This model gives excellent predictions of $c_s^{(\Delta)}$ and its dependence upon stability and height.

1. Introduction

Three-dimensional simulations of atmospheric boundary layer (ABL) flows at high Reynolds numbers are feasible only on computational grids with a spacing substantially larger than the Kolmogorov scale. In a large-eddy simulation (LES; see, e.g., Deardorff 1970; Moeng 1984; Mason 1994; Lesieur and Métais 1996) the transport equations resolve all scales of motion larger than the grid size Δ. Scale separation is achieved through low-pass spatial filtering, which defines the ''resolved'' or ''filtered'' velocity as

$$\tilde{\mathbf{u}}(\mathbf{x}) = \int \mathbf{u}(\mathbf{x}')F_\Delta(\mathbf{x} - \mathbf{x}')\, d\mathbf{x}'. \quad (1)$$

Here, F_Δ is the (homogeneous) filter function for a scale Δ. Subgrid scales (smaller than Δ) are parameterized using subgrid-scale (SGS) models. The SGS model is crucial for an LES to generate realistic turbulent fields in the ABL, especially in regions where the local integral scale is smaller than the filter scale Δ. SGS models parameterize the SGS stress τ_{ij}, whose divergence enters the filtered Navier–Stokes equations. The SGS stress,

$$\tau_{ij} = \widetilde{u_i u_j} - \tilde{u}_i\tilde{u}_j, \quad (2)$$

is expressed in terms of velocity gradients by the Smagorinsky model (Smagorinsky 1963):

$$\tau_{ij}^{\text{Smag}} - \frac{1}{3}\tau_{kk}\delta_{ij} = -2\nu_T\tilde{S}_{ij}, \qquad \nu_T = (c_s^{(\Delta)}\Delta)^2|\tilde{S}|, \quad (3)$$

where $\tilde{S}_{ij}$ is the strain-rate tensor, $|\tilde{S}| = \sqrt{2\tilde{S}_{ij}\tilde{S}_{ij}}$ is its magnitude, and ν_T is the eddy viscosity. When this closure is used in a traditional LES, $c_s^{(\Delta)}$ needs to be specified a priori.

It has often been remarked (Pope 2000; Meneveau 1994) that a single value of $c_s^{(\Delta)}$ cannot simultaneously yield the correct SGS dissipation, SGS stress, and the correct divergence of the stress (SGS force). Moreover, it is well known that the SGS stress tensor is not deterministically aligned with the rates of strain and that at a local level the Smagorinsky closure is highly unrealistic (Bardina et al. 1980; McMillan and Ferziger

Corresponding author address: Charles Meneveau, JHU, 3400 N. Charles St., Baltimore, MD 21218-2681.
E-mail: meneveau@jhu.edu

1979; Liu et al. 1994; Bastiaans et al. 1998; Higgins et al. 2003). Despite these limitations, the eddy-viscosity closure is still the most widely used SGS model in atmospheric and engineering applications. The present study focuses on how to dynamically obtain the model coefficient, which directly affects the rate of SGS energy dissipation.

Once the eddy-viscosity closure is accepted, the Smagorinsky coefficient $c_s^{(\Delta)}$ has to be chosen appropriately. Its magnitude determines the rate of kinetic energy dissipation due to the SGS model. This SGS dissipation rate Π_Δ is defined according to $\Pi_\Delta = -\langle \tau_{ij}\tilde{S}_{ij}\rangle$. The dissipation predicted by the Smagorinsky model, $\Pi_\Delta^{\text{Smag}} = -\langle \tau_{ij}^{\text{Smag}}\tilde{S}_{ij}\rangle$ depends upon $c_s^{(\Delta)}$ and on the variance of the resolved strain-rate tensor. Typically, the resolved turbulence levels will be damped excessively if $c_s^{(\Delta)}$ is too large; conversely, if $c_s^{(\Delta)}$ is too small, energy pileup occurs at the smallest resolved scales of the turbulence. This leads to anomalous statistics and can result in numerical instabilities when a poor numerical method is used.

In a traditional LES of atmospheric boundary layers, $c_s^{(\Delta)}$ is deduced from phenomenological theories of turbulence (Lilly 1967; Mason 1994). Stability dependence of $c_s^{(\Delta)}$ has traditionally been derived from theoretical models for the energy spectra (Hunt et al. 1988; Deardorff 1980; Canuto and Cheng 1997). These studies result in expressions relating $c_s^{(\Delta)}$ with parameters characterizing the atmospheric stability (such as the Richardson number or Obukhov length L); typically, the characteristic length scale $c_s^{(\Delta)}\Delta$ is found to decrease in stable conditions. Redelsperger et al. (2001) derive an expression for the eddy-viscosity length scale as function of height and stability from experimental observations of energy spectra in blocked turbulence. A direct empirical method to determine $c_s^{(\Delta)}$ and its dependence upon physical flow parameters from field experimental data was proposed in Porté-Agel et al. (2001a,b), which expanded on earlier work of Porté-Agel et al. (1998, 2000b) and Tong et al. (1999). Data from two linear arrays of sonic anemometers placed perpendicularly to the flow in the ABL (Tong et al. 1998; Porté-Agel et al. 2001a) were used to determine SGS model coefficients (for details, see section 2b). Among others, Porté-Agel et al. (2001b) confirm from the data that the Smagorinsky coefficient $c_s^{(\Delta)}$ depends on height z, filter scale Δ, and atmospheric stability. In particular, $c_s^{(\Delta)}$ decreases for small z/Δ. In a more detailed, recent study of the Smagorinsky coefficient, Kleissl et al. (2003, hereafter KMP) analyzed nearly 160 h of data from the Horizontal Array Turbulence Study (HATS), a field experiment in the ABL with 14 sonic anemometers in two arrays. KMP quantified the decrease of $c_s^{(\Delta)}$ with stability and proximity to the ground and proposed an empirical relationship for $c_s^{(\Delta)}$ as a function of Δ/z and Δ/L. Sullivan et al. (2003) find that the measured values of $c_s^{(\Delta)}$ collapse quite well when Λ_w, the length scale at the peak of the spectrum of vertical velocity, is used to scale the filter size. In LES, parameterization of $c_s^{(\Delta)}$ as a function of Λ_w/Δ is feasible if Λ_w is known a priori or it can be determined from energy spectra that are computed in space (such as in LES with homogeneous boundary conditions). Still, such parameterizations require knowing empirical formulas for the coefficient as function of Λ_w/Δ. In other words, even if one can obtain Λ_w from the simulation's spectra during an LES, a functional form for $c_s^{(\Delta)}$ as function of Λ_w must be prescribed, with an associated need for empirical coefficients. Along a fundamentally different line of thinking, Germano et al. (1991) proposed the ''dynamic model.'' Instead of prescribing $c_s^{(\Delta)}$ a priori as a function of flow parameters, this approach is based upon the idea of analyzing the statistics of the simulated large-scale field (during an LES) to determine the undetermined model parameters. The dynamic model is based on the Germano identity (Germano 1992),

$$L_{ij} \equiv \widetilde{\overline{u}_i\overline{u}_j} - \widetilde{\overline{u}}_i\widetilde{\overline{u}}_j = T_{ij} - \widetilde{\tau_{ij}}. \tag{4}$$

In the preceding, L_{ij} is the resolved stress tensor and $T_{ij} = \widetilde{\overline{u_i u_j}} - \widetilde{\overline{u}_i}\widetilde{\overline{u}_j}$ is the stress at a test-filter scale $\alpha\Delta$ [an overline $\overline{(\,.\,.)}$ denotes test filtering at a scale $\alpha\Delta$]. If one applies this dynamic procedure by replacing T_{ij} and τ_{ij} by their prediction from the basic Smagorinsky model the result is

$$L_{ij} - \frac{1}{3}\delta_{ij}L_{kk} = (c_s^{(\Delta)})^2 M_{ij},$$

where

$$M_{ij} = 2\Delta^2\left(\overline{|\tilde{S}|\tilde{S}_{ij}} - \frac{(\alpha\Delta c_s^{(\alpha\Delta)})^2}{(\Delta c_s^{(\Delta)})^2}\overline{|\tilde{S}|}\,\overline{\tilde{S}_{ij}}\right). \tag{5}$$

To proceed, the crucial assumption in the standard dynamic model (Germano et al. 1991) is scale invariance of the coefficient, namely,

$$c_s^{(\Delta)} = c_s^{(\alpha\Delta)}. \tag{6}$$

This step allows the only remaining unknown parameter in Eq. (5), $c_s^{(\Delta)}$, to be obtained. The overdetermined system of equations can be solved by minimizing the square error averaged over all independent tensor components (Lilly 1992), and some spatial domain (Ghosal et al. 1995) or temporal domain (Meneveau et al. 1996). The result is

$$(c_s^{(\Delta)})^2 = \frac{\langle L_{ij}M_{ij}\rangle}{\langle M_{ij}M_{ij}\rangle}. \tag{7}$$

Here the symbol $\langle\,.\,.\rangle$ denotes ensemble, time or spatial averaging, depending on the context. In the derivation [Eqs. (5)–(7)] we ignored that $c_s^{(\Delta)}$ is a function of position [see Ghosal et al. (1995) for a discussion of the resulting integral equation]. The dynamic model has been successfully applied to a variety of engineering flows [see Meneveau and Katz (2000) and Piomelli (1999) for reviews]. In general, it provides realistic pre-

dictions of $c_s^{(\Delta)}$ when the flow field is sufficiently resolved, that is, the test-filter scale $\alpha\Delta$ is smaller than the local integral scale of turbulence.

In the context of ABL turbulence the dynamic Smagorinsky model has been implemented in an LES by Porté-Agel et al. (2000a). They examined the scale-invariance hypothesis and the dynamic model with an LES of a neutral ABL. They found that near the wall streamwise energy spectra decay too slowly, indicating that the dynamically determined coefficient is too small. In addition, by running four simulations at different resolutions they demonstrated a clear scale-dependence of the Smagorinsky coefficient ($c_s^{(\Delta)} \neq c_s^{(\alpha\Delta)}$), which violates the scale-invariance assumption of the dynamic model [Eq. (6)]. As a consequence, Porté-Agel et al. (2000a) proposed a scale-dependent dynamic model. In addition to a test filter at $\alpha\Delta$, a test filter at $\alpha^2\Delta$ (denoted by a hat below) delivers another equation similar to Eq. (5):

$$Q_{ij} - \frac{1}{3}\delta_{ij}Q_{kk} = (c_s^{(\Delta)})^2 N_{ij},$$

where

$$Q_{ij} = \widehat{\tilde{u}_i\tilde{u}_j} - \widehat{\tilde{u}}_i\widehat{\tilde{u}}_j \quad \text{and} \tag{8}$$

$$N_{ij} = 2\Delta^2\left(\widehat{|\tilde{S}|\tilde{S}}_{ij} - \frac{(\alpha^2\Delta c_s^{\alpha^2\Delta})^2}{(\Delta c_s^{(\Delta)})^2}\widehat{|\tilde{S}|\tilde{S}}_{ij}\right). \tag{9}$$

With this additional equation the scale-invariance assumption can be relaxed. A new parameter β is defined according to

$$\beta = \frac{(c_s^{(\alpha\Delta)})^2}{(c_s^{(\Delta)})^2}. \tag{10}$$

Under the assumption that β does not depend on scale, Eqs. (5) and (9) can be solved for the two unknowns, $c_s^{(\Delta)}$ and β (Porté-Agel et al. 2000a). Note that this assumption is equivalent to assuming a power-law behavior $(c_s^{(\Delta)})^2 \sim \Delta^{\Phi}$, or dimensionally appropriate,

$$(c_s^{(\alpha\Delta)})^2 = (c_s^{(\Delta)})^2\alpha^{\Phi}. \tag{11}$$

For details on the computation of β see the appendix. It needs to be emphasized that β is determined dynamically from the resolved scales; the power-law behavior in Eq. (11) is the only empirical assumption. Porté-Agel et al. (2000a) applied the scale-dependent dynamic SGS model to an LES of a neutral boundary layer and obtained good agreement with observations for mean velocity gradients and streamwise energy spectra.

The objective of the present study is to examine field data at various length scales and determine whether the dynamic model yields realistic predictions of the coefficient $c_s^{(\Delta)}$ and its dependencies upon distance to the ground and atmospheric stability. Both the scale-invariant (Germano et al. 1991) and the more elaborate scale-dependent forms (Porté-Agel et al. 2000a) of the dynamic model will be examined. Note that a priori tests do not always give the same results as those obtained in LES numerical implementations. In LES numerical discretization errors and feedback of the SGS model on the resolved scales can affect the results. A forthcoming paper by the authors will examine the applicability of a priori results from the present paper to LES in more detail. The current paper uses the same field data as KMP, but the data are processed at a different set of length scales to perform the various filtering operations required for the dynamic models. We also investigate how the averaging time scale influences the results. As indicated in Eq. (7) the dynamic model requires averaging of data. Knowledge of an appropriate averaging time scale is relevant for the Lagrangian SGS model (Meneveau et al. 1996), which determines the model coefficient by accumulating weighted averages over fluid path lines. However, due to the experimental conditions, only Eulerian averaging can be used in this study.

The present paper is organized as follows. In section 2, we describe the field experiment and the data processing techniques. Section 2 also contains a brief review of the results of KMP: measured distributions of $c_s^{(\Delta)}$ as function of height and stratification. Section 3 studies the ability of the scale-invariant dynamic and scale-dependent dynamic SGS models to reproduce the behavior of $c_s^{(\Delta)}$. Conclusions are presented in section 4.

2. Dataset and processing

a. The HATS dataset

In HATS two vertically displaced horizontal arrays of 14 Campbell Scientific three-component sonic anemometer–thermometers (CSAT3) were installed in the atmospheric surface layer in the San Joaquin Valley close to Kettlemen City, California, from 31 August until 1 October 2000. The HATS experiment was described in detail in KMP (Kleissl et al. 2003) and Horst et al. (2004). The focus of KMP was to determine relationships between $c_s^{(\Delta)}$ and different relevant length scales: height above ground z, filter scale Δ, and the Obukhov length L. Parameter L is defined as

$$L = \frac{-u_*^3}{\kappa\frac{g}{\theta_o}\langle w'\theta'\rangle}, \tag{12}$$

where $u_* = (-\langle u'w'\rangle)^{1/2}$ is the friction velocity, θ_0 is the mean air temperature, g is the gravitational acceleration, and $\kappa = 0.4$ is the von Kármán constant. Data from two sensor setups were used to dynamically determine the Smagorinsky coefficients. These setups are presented in Table 1.

Figure 1 shows a schematic of the instrument setup for arrays 1 and 2. To compute SGS quantities, the velocity fields have to be spatially filtered in two dimensions at a scale Δ. Since the velocities will also be filtered at two larger scales, $\alpha\Delta$ and $\alpha^2\Delta$, Δ is chosen to be smaller than the values used in KMP. Here we use

TABLE 1. Array properties for the HATS experiment. Here, d = double-filtered array; s = single-filtered array; d_0 = displacement height; δ_y = lateral instrument spacing; Δ = filter size.

Array No.	Data (h)	$z_d - d_0$ (m)	$z_s - d_0$ (m)	δ_y (m)	Δ (m)	$\frac{\Delta}{z_d - d_0}$ (−)	$\langle u_d \rangle$ (m s^{-1})
1	46.0	3.13	6.58	3.35	6.70	2.1	2.46
2	38.7	4.01	8.34	2.17	4.34	1.1	2.72

twice the lateral instrument spacing as the basic filter length, that is, $\Delta = 2\delta_y$, where δ_y is the lateral spacing of the sonic anemometers. As in Sullivan et al. (2003) and Horst et al. (2004), convolutions with the top-hat filter of width Δ are evaluated using the trapezoidal integration rule. This is equivalent to using discrete weights $(0.5, 1, \ldots, 1, 0.5)/(n-1)$ for data from n sensors spaced in the lateral (y) direction. Note that other options exist to define weights for discretely sampled data. For instance, Vasilyev et al. (1998) use the second moment of the filter's discrete Fourier transfer function to relate filter width with the weights. The difference among these methods is not large when considering the compounded two-dimensional filtering: in the streamwise direction, the filtering occurs on the much finer time-sampling grid (see later), and thus there is negligible ambiguity how to relate filter width and weight factors. This streamwise filter is responsible for removing most of the SGS variance, rendering the effects of the less accurate cross-stream filters less important. A smooth Gaussian filter is used in the streamwise (x) direction, where 20-Hz sampling results in a higher resolution with a spacing of 0.05 s $\langle u \rangle$ m s^{-1} $\approx$ 0.13 m, using Taylor's hypothesis. The Fourier transform of the Gaussian filter function $\hat{G}_\Delta = \exp[-(k_1^2\Delta^2/24)]$ is multiplied with the Fourier transform of each 8192 data points segment ($\sim$6.8 min) of the velocity time series. Before the convolution, the mean of the velocity time series is subtracted and a Bartlett window is applied. Derivatives are computed from the filtered time series. Due to edge effects of the filter and the streamwise derivative, a segment of duration $(\alpha^2\Delta/2 + \delta_x)/\langle u_d \rangle$ is discarded from beginning and end of the time series of all filtered variables. Then averages for various time scales T_c are computed. For an analysis of filter accuracy, see Horst et al. (2004) and Cerutti and Meneveau (2000).

Gradients are calculated with finite differences (FDs). In the vertical direction ($x_3 = z$), the setup necessitates a first-order one-sided FD $\partial\tilde{u}/\partial z|_{z_d} = (z_s - z_d)^{-1}[\tilde{u}(z_s) - \tilde{u}(z_d)]$. In the horizontal directions, a second-order centered FD scheme is used, for example, for the y direction: $\partial\tilde{u}_i/\partial y|_{y0} = (2\delta_y)^{-1}[\tilde{u}_i(y_0 + \delta_y) - \tilde{u}_i(y_0 - \delta_y)]$. Assuming Taylor's hypothesis, the same formula with $\delta_x = \delta_y$ is used in the streamwise direction to compute $\partial\tilde{u}_i/\partial x$.

In order to depict the available data as a function of stability and array, KMP divided the data into segments

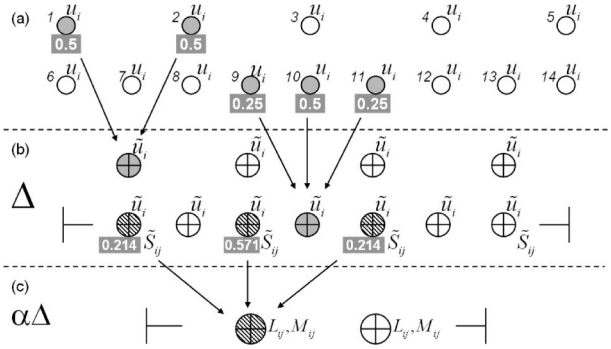

FIG. 1. Experimental setup of HATS. Three-dimensional sonic anemometers are displayed as circles. The reference number of the instrument is to the upper left and the measured or computed variable at this location is to the right. (a) Unfiltered variables. Sample lateral filter weights for a scale Δ are marked in gray below locations 1–2 and 9–11. (b) Variables filtered at scale Δ. Sample lateral filter weights are displayed below locations 7, 9, and 11, which are hatched. (c) Variables filtered at scale 1.75Δ.

of length 6.8 min. These segments were classified according to stability, characterized in terms of Obukhov length L, defined as in Eq. (12) and yielding a dimensionless parameter Δ/L. The distribution of data by stability can be seen in KMP's Fig. 2 for various heights (characterized in terms of Δ/z). In the present paper we use the same procedure and data classification. In the following the procedures to compute the model coefficient will be described in more detail.

b. *Empirically determined Smagorinsky coefficient: Procedures and results*

The Smagorinsky coefficient is measured from the field data by matching mean measured and modeled SGS dissipations Π_Δ (Clark et al. 1979; KMP),

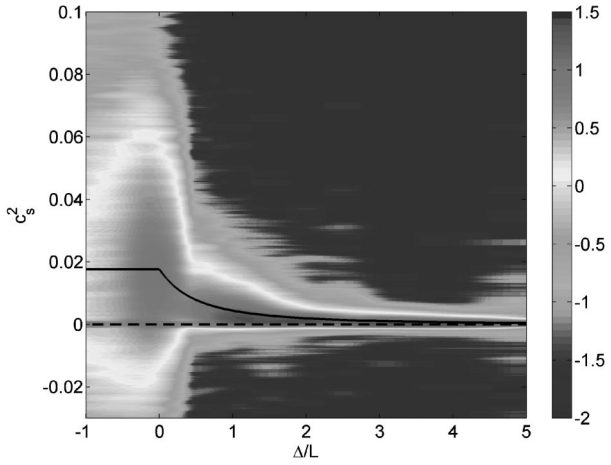

FIG. 2. Contour plots of conditional PDF of $(c_s^{\Delta,\mathrm{emp}})^2$, $P(c_s^2|\Delta/L)$, for array 2 ($\Delta/z \sim 1.1$). The contours show $\log_{10}P(c_s^2|\Delta/L)$. The averaging time to compute $c_s^{(\Delta)}$ is $T_c = 3.2$ s $\sim 2.0\Delta/\langle u \rangle$. The solid line is the empirical fit of Eq. (14). The dashed line shows $(c_s^\Delta)^2 = 0$.

$$(c_s^{(\Delta,\mathrm{emp})})^2 = -\frac{\langle \tau_{ij}\tilde{S}_{ij}\rangle}{\langle 2\Delta^2|\tilde{S}|\tilde{S}_{ij}\tilde{S}_{ij}\rangle}, \quad (13)$$

where $\langle\ \rangle$ denotes Eulerian time averaging of HATS data over a time scale T_c. KMP analyzed the behavior of $c_s^{(\Delta,\mathrm{emp})}$ from HATS data as function of parameters Δ/z and Δ/L. It was found that the data can be described by a function of the form:

$$c_s^{(\Delta,\mathrm{emp})} = c_0\left[1 + \frac{c_0}{\alpha}R\left(\frac{\Delta}{L}\right)\right]^{-1}\left[1 + \left(\frac{c_0}{\kappa}\frac{\Delta}{z}\right)^n\right]^{-1/n}. \quad (14)$$

Here, R is the ramp function. The parameters of Eq. (14) were determined as $n = 3$ and $\alpha = c_0 = 0.135$.

In the present paper, the filter size is half of that in KMP. Figure 1a provides a sketch of the filtering procedures in the transverse (y or x_2) direction. A three-point top-hat filter with trapezoidal weights [0.25, 0.5, 0.25] is used in the lower array and a two-point filter with weights [0.5, 0.5] is used in the upper array. In the streamwise direction, the Gaussian filter is used as described in the preceding section. Thus filtered velocities $\tilde{u}_i$, and SGS stresses τ_{ij}, at a scale $\Delta = 2\delta_y$ are available at locations 7–13 and between locations 1 and 5 (Fig. 1b). As a result, the filtered strain-rate tensors can be obtained at locations 9 and 11, using a second-order centered FD in the horizontal and first-order one-sided FD in the vertical directions, respectively. Since τ_{ij} is available at these locations as well, the Smagorinsky coefficients $c_s^{(\Delta,\mathrm{emp})}$ are evaluated at locations 9 and 11. The results from these two locations are essentially identical and only results from location 9 are presented.

A first question to address is whether the data analyzed at scale $\Delta = 2\delta_y$ provide results that are consistent with those of KMP that were obtained at a larger scale, using more sensors from each array. To compare our results with KMP, data from array 2 ($\Delta/z \sim 1.1$) are divided into stability bins from $\Delta/L = -1$ to $\Delta/L = 5$ and further divided into subsegments of length $T_c = 3.2$ s. This corresponds roughly to a length scale $T_c\langle u\rangle \sim 8.7$ m, which is on the order of twice the filter scale $\Delta \sim 4.3$ m. The empirically determined Smagorinsky model coefficient $c_s^{(\Delta,\mathrm{emp})}$ is obtained by evaluating the averages in Eq. (13) over time T_c. In order to isolate the dependence on Δ/L, we compute the conditional PDF of $(c_s^{\Delta,\mathrm{emp}})^2$, $P(c_s^2\,|\,\Delta/L) = P(c_s^2, \Delta/L)/P(\Delta/L)$, where $P(\Delta/L)$ is the fraction of data contained in each Δ/L bin. The $(c_s^{\Delta})^2$ range $[-0.03 < (c_s^{\Delta})^2 < 0.1]$ is divided into 260 bins. Figure 2 shows the conditional PDF of $(c_s^{\Delta,\mathrm{emp}})^2$ using color contours. The figure confirms the results of KMP: $c_s^{\Delta,\mathrm{emp}}$ decreases in stable conditions and its PDF shows a large spread in unstable conditions with a considerable number of negative values. The most likely value of $c_s^{(\Delta,\mathrm{emp})}$ corresponds well to the empirical fit of KMP. Liu et al. (1995) obtained the eddy-viscosity field without averaging and also found a highly variable eddy-viscosity field with negative values, which causes numerical instabilities in LES.

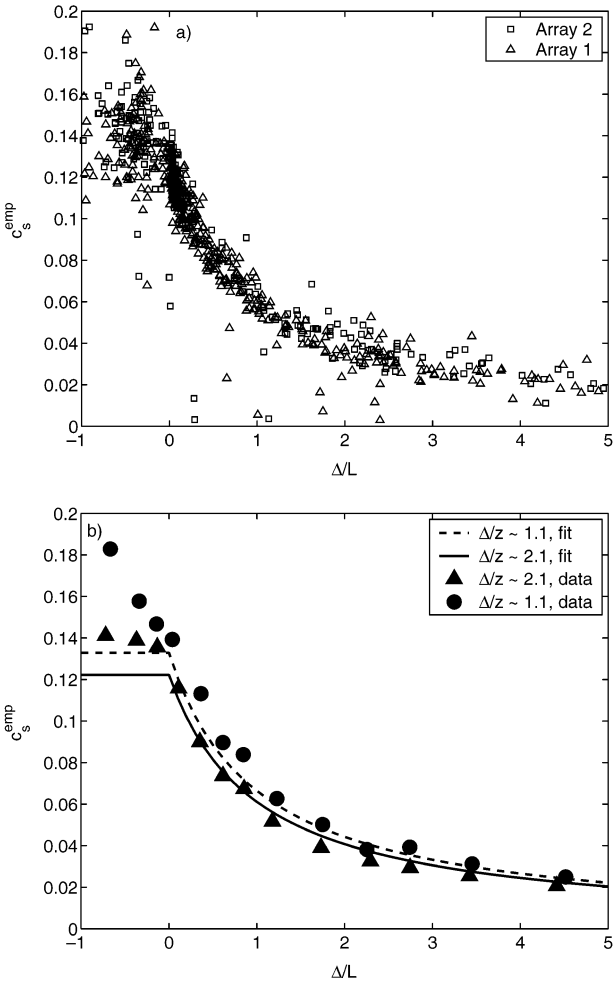

FIG. 3. (a) Comparison of $c_s^{(\Delta,\mathrm{emp})}$ from array 1 of the present paper ($z = 3.13$ m, $\Delta = 6.7$ m) with $c_s^{(\Delta,\mathrm{emp})}$ from array 2 of Kleissl et al. (2003) ($z = 4.01$ m, $\Delta = 8.68$ m). The averaging time is $T_c = 6.8$ min. (b) Comparison of $c_s^{(\Delta,\mathrm{emp})}$ from the present paper (symbols) with empirical fits of Kleissl et al. (2003) mentioned in Eq. (14). Parameter $c_s^{(\Delta,\mathrm{emp})}$ is obtained from Eq. (13) by averaging over the total time in each stability bin.

The comparison with KMP is repeated using a larger averaging time scale T_c. Figure 3a shows a direct comparison of data from array 1 ($\Delta/z \sim 2.1$) of the present paper with data from a better-resolved filter but same Δ/z from array 2 of KMP for an averaging time scale of $T_c = 6.8$ min. The results agree very well, even though they are obtained from two different arrays. The agreement confirms that the curves collapse for a given Δ/z, independent of the dimensional values of Δ or z. Finally, in Fig. 3b we perform a comparison based on the global time averages of SGS dissipations. Here we average the terms in Eq. (13) over all data available in each Δ/L bin, obtaining a single measured value of $c_s^{(\Delta,\mathrm{emp})}$ in each bin. The coefficients are very close to the lines that are the predictions from the fit of KMP.

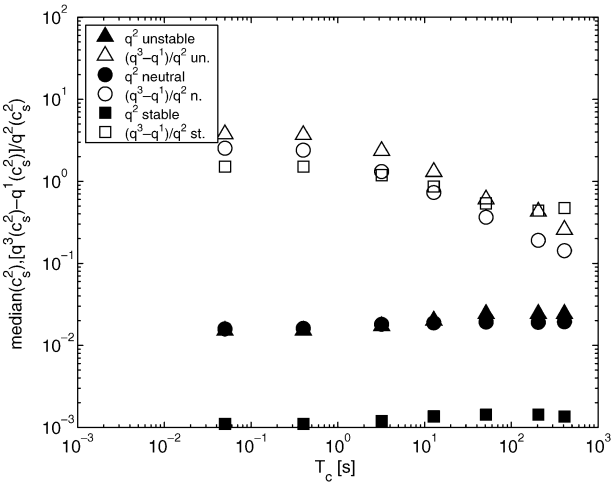

FIG. 4. Median q^2 and spread $(q^3 - q^1)/q^2$ of the $(c_s^{\Delta,\mathrm{emp}})^2$ distribution as a function of averaging time scale T_c for different stabilities: unstable ($-0.5 < \Delta/L < -0.25$), near neutral ($0 < \Delta/L < 0.25$), and stable ($2 < \Delta/L < 2.5$). The data are from array 2.

Only in unstable conditions are the predictions about ~10% too small. Besides confirming the collapse of the data, this comparison shows that the coarser filter resolution in the lateral direction (using only two or three sensors) does not affect the prediction of $c_s^{(\Delta)}$.

To provide a systematic description of the effects of averaging time T_c upon the statistics of $c_s^{(\Delta,\mathrm{emp})}$, the main aspects of the PDF of $c_s^{(\Delta,\mathrm{emp})}$ are documented as functions of T_c. Figure 4 displays the median of $c_s^{(\Delta,\mathrm{emp})}$ as a function of T_c for different stabilities. As reported in KMP, the median of $c_s^{(\Delta,\mathrm{emp})}$ is constant with averaging time and much smaller in stable conditions than in unstable and neutral conditions. In unstable conditions the median increases slightly with averaging time. A measure of the spread of the PDF is documented in terms of the difference between third and first quartile normalized by the second quartile. As expected, this measure decreases with increasing T_c, in neutral and unstable conditions. As reported in KMP, the decrease is weaker in stable conditions, which can be attributed to larger intermittency in stable conditions.

c. Scale-invariant dynamic model: Procedures

In order to obtain the dynamic model coefficient from Eq. (7), filtered strain-rate tensors and velocity vectors at a scale Δ have to be filtered at $\alpha\Delta$ to evaluate L_{ij} and M_{ij}. Usually $\alpha = 2$, but the limited maximum filter width in the lateral direction requires us to use $\alpha = 1.75$ in the present study. As shown in Germano et al. (1991), the sensitivity of the dynamic coefficient to α is not expected to be important. Figure 1b shows that $\tilde{S}_{ij}$ at a scale Δ can be obtained at locations 7, 9, 11, and 13. At locations 9 and 11 $\tilde{S}_{ij}$ is computed from centered horizontal FD and one-sided vertical FD. At locations 7 and 13, the horizontal and the vertical FDs are one-sided. A filter of size 1.75Δ is applied to $\tilde{u}_i$, $\tilde{S}_{ij}$, $|\tilde{S}|$, and $|\tilde{S}|\tilde{S}_{ij}$. The filter weight w_i associated with a variable (already filtered at scale Δ) at location y_i, used to compute a test-filtered variable at location $y_{\alpha\Delta}$, is evaluated as follows: $w_i^* = |[y_i - \Delta/2, y_i + \Delta/2] \cap [y_{\alpha\Delta} - \alpha\Delta/2, y_{\alpha\Delta} + \alpha\Delta/2]|$, where $[y_i - \Delta/2, y_i + \Delta/2]$ is the segment of length Δ surrounding the point y_i, and $[y_{\alpha\Delta} - \alpha\Delta/2, y_{\alpha\Delta} + \alpha\Delta/2]$ is the segment of length $\alpha\Delta$ surrounding the point $y_{\alpha\Delta}$. Variables y_i and $y_{\alpha\Delta}$ are the y coordinates of the instrument at location i and the test-filtered variable, respectively. Weights w_i^* are normalized so that they sum up to 1: $w_i = w_i^*/\Sigma_i\, w_i^*$. This procedure gives weights of $w_i = [0.214, 0.571, 0.214]$ for locations $i = [7, 9, 11]$ and $i = [9, 11, 13]$. Using the test-filtered variables, the time series of $L_{ij}M_{ij}$ and $M_{ij}M_{ij}$ are computed at locations 9 and 11, averaged over a time scale T_c, and divided to obtain $c_s^{(\Delta,\mathrm{dyn})}$ using Eq. (7). Note that in defining α, we follow the prevalent usage in practical implementations of the dynamic model of not taking into account the effects of compound filtering (see, however, Najjar and Tafti 1996 for a discussion of effects of compound filters and a quantification of its effects on LES using the dynamic model).

d. Scale-dependent dynamic model: Procedures

The scale-dependent dynamic coefficient is obtained similarly to procedures described in section 2c. The filtered strain-rate tensors and filtered velocity vectors of Fig. 1b are now, however, filtered at $\alpha^2\Delta = 1.75^2\Delta$. The same weighting scheme as in section 2c produces weights of $w_i = [0.18, 0.32, 0.32, 0.18]$ for strain-rate tensors at locations [7, 9, 11, 13]. The resulting $\widehat{|\tilde{S}|\tilde{S}_{ij}}$, and $\widehat{|\tilde{S}|\tilde{S}_{ij}}$ are used to compute N_{ij}, while $\widehat{\tilde{u}_i\tilde{u}_j}$ and $\hat{\tilde{u}}_i$ are used to compute Q_{ij}.

It is important to note that N_{ij} is a function of β. Parameter β is computed using procedures identical to those in Porté-Agel et al. (2000a, hereafter POR). Six coefficients of a fifth-order polynomial in β are obtained from averaging products of strain rates and resolved stresses over T_c, as described in the appendix [Eqs. (A2)–(A10)]. Then the roots of the polynomial in β are determined by the ''roots'' function in MATLAB (The Mathworks Inc.). As argued in POR, only the largest real root is physically meaningful. A time series of Q_{ij} and N_{ij} is obtained from Eq. (9) using the β value derived from quantities averaged over T_c. Finally, the scale-dependent dynamic procedure yields the coefficient at a scale Δ as $(c_s^{(\Delta,\mathrm{sd-dyn})})^2 = \langle Q_{ij}N_{ij}\rangle/\langle N_{ij}N_{ij}\rangle$.

3. Smagorinsky coefficients determined from dynamic SGS models

a. Scale-invariant dynamic model: Results

To begin, the scale-invariant, dynamically determined Smagorinsky model coefficient $c_s^{(\Delta,\mathrm{dyn})}$ is obtained according to section 2c by evaluating the averages over

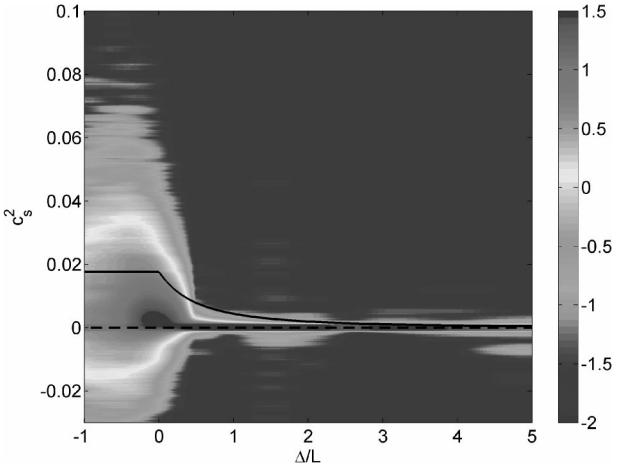

FIG. 5. Contours plots of the PDF of $(c_s^{\Delta,\mathrm{dyn}})^2$ conditioned on Δ/L for array 2 ($\Delta/z \sim 1.1$). The contours show $\log_{10}P(c_s^2 \mid \Delta/L)$. The averaging time to compute $c_s^{(\Delta)}$ is $T_c = 3.2$ s $\sim 2.0\Delta/\langle u\rangle$. The solid line is the empirical fit of Eq. (14). The dashed line shows $(c_s^{\Delta})^2 = 0$.

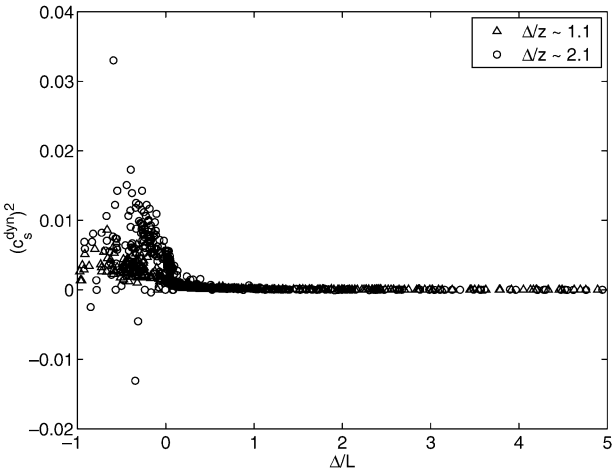

FIG. 6. Smagorinsky coefficient $c_s^{(\Delta,\mathrm{dyn})}$ as a function of Δ/L for arrays 1 and 2 and an averaging time of $T_c = 6.8$ min.

time $T_c = 3.2$ s for array 2. Figure 5 shows the PDF of $(c_s^{(\Delta,\mathrm{dyn})})^2$ conditioned on Δ/L using color contours. It is apparent that the most likely value of $(c_s^{(\Delta,\mathrm{dyn})})^2$ depends on stability. It is very close to zero for $\Delta/L > 1$ and increases strongly in near-neutral conditions ($\Delta/L \sim 0$). In neutral and unstable conditions, the spread in the PDF is large with a considerable number of negative values. These trends are consistent with those of the empirical coefficient reported in section 2b. However, comparing the color contours with the line from the fit in Eq. (14) and with the conditional PDF of $c_s^{(\Delta,\mathrm{emp})}$ in Fig. 2, it can be seen that the dynamically determined coefficients are too small, especially in conditions of stable stratification ($\Delta/L > 0$).

Figure 6 shows the empirically and dynamically determined coefficient for a longer averaging time $T_c = 6.8$ min and for arrays 1 and 2. At this averaging scale too, the results confirm that the dynamic model predicts a coefficient that is significantly smaller than $c_s^{(\Delta,\mathrm{emp})}$. Finally, the same results are obtained when performing the averages over all available data as shown in Fig. 7, where one value of $c_s^{(\Delta,\mathrm{dyn})}$ is plotted for each Δ/L bin.

The dynamic procedure predicts the correct basic trends of the coefficient with stability (Δ/L) and height (Δ/z), but the magnitudes of the coefficients are too small by significant factors. In unstable and neutral conditions, factors range from 2 to 5. In very stable conditions this factor is as large as an order of magnitude or more. Thus, the energy transfer (Π_Δ) from resolved scales to SGS is too small, and in an LES using such a model one would expect a high-wavenumber pileup of energy in the spectra near the wall. This weakness of the dynamic model was already observed in an LES of the ABL (POR) in neutral conditions, and present results suggest that this weakness would be exacerbated in conditions of stable stratification.

The variability of $c_s^{(\Delta,\mathrm{dyn})}$ is examined in Fig. 8 by plotting the quartiles of the $(c_s^{\Delta,\mathrm{dyn}})^2$ distribution for different averaging times T_c. The median of $c_s^{(\Delta,\mathrm{dyn})}$ is very similar for T_c ranging from 0.05 s (no averaging) to hours. The relative spread of the PDF decreases with averaging time, which agrees with results from KMP and Fig. 4 for $c_s^{(\Delta,\mathrm{emp})}$.

In summary, the results for $c_s^{(\Delta,\mathrm{dyn})}$ consistently show that the dynamic procedure underpredicts the Smagorinsky coefficient when Δ is close to, or exceeds, L or z, or both. This deficiency is not surprising. As suggested by the same empirical fit through the available data for $c_s^{(\Delta,\mathrm{emp})}$ [Eq. (14)], for any fixed value of z or L the coefficient is dependent upon Δ unless $\Delta \ll L$ and $\Delta \ll z$. Thus, the expected behavior of the coefficient contradicts the basic assumption of scale invariance underlying the dynamic model. This was already noted in POR for the neutral case but $\Delta > z$. The scale-dependent dynamic model described in section 2d addresses this

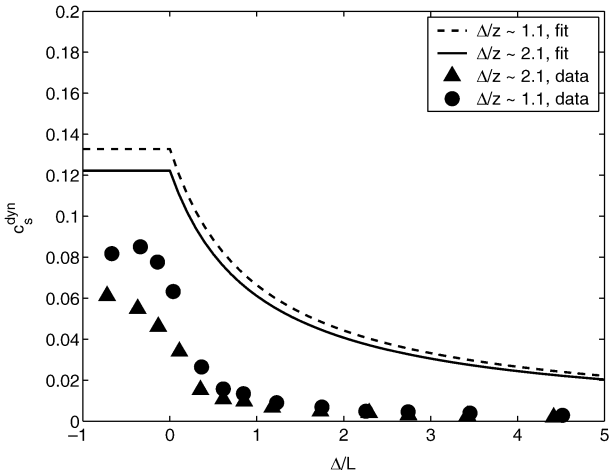

FIG. 7. Comparison of $c_s^{(\Delta,\mathrm{dyn})}$ (symbols) with empirical fits for $c_s^{(\Delta,\mathrm{emp})}$ of Kleissl et al. (2003) [Eq. (14)]. Variables are averaged over all segments in each stability bin.

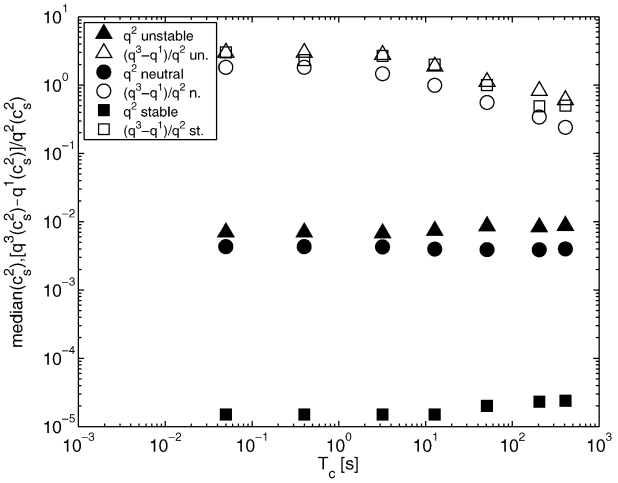

FIG. 8. Median q^2 and spread $(q^3 - q^1)/q^2$ of the $(c_s^{\Delta,\mathrm{dyn}})^2$ distribution as a function of averaging time scale T_c for different stabilities: unstable ($-0.5 < \Delta/L < -0.25$), near neutral ($0 < \Delta/L < 0.25$), and stable ($2 < \Delta/L < 2.5$). The data are from array 2.

problem. In the following section we analyze the data to study whether the scale-dependent model yields more realistic predictions of the coefficient compared to the standard dynamic model.

b. Scale-dependent dynamic model: Results

Analysis for the scale-dependent dynamic model first requires computation of the parameter describing scale dependence of the Smagorinsky coefficient, $\beta = (c_s^{\alpha\Delta})^2/(c_s^{\Delta})^2$. Again, data from array 2 ($\Delta/z \sim 1.1$) are divided into bins of different stabilities ranging from $\Delta/L = -1$ to $\Delta/L = 5$, and divided into subsegments of length T_c. Parameter β is obtained according to section 2d. Specifically, we use Eqs. (A2)–(A10). Averages such as

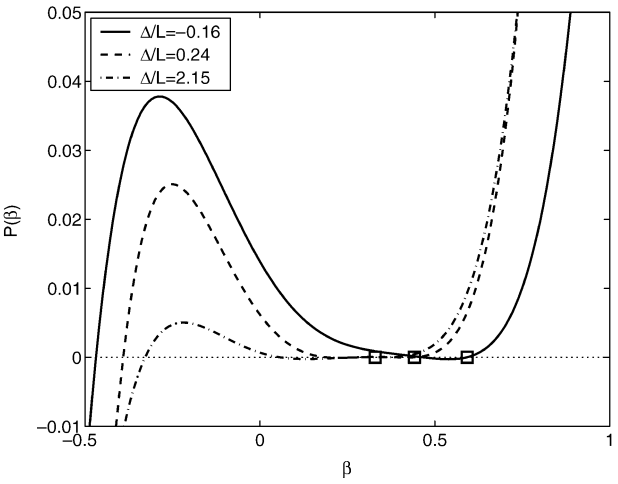

FIG. 9. Representative fifth-order polynomials $P(\beta)$ from Eq. (A2) for different stabilities and $\Delta/z \sim 1.1$. The squares mark the largest roots $\beta = 0.593$, 0.442, and 0.330.

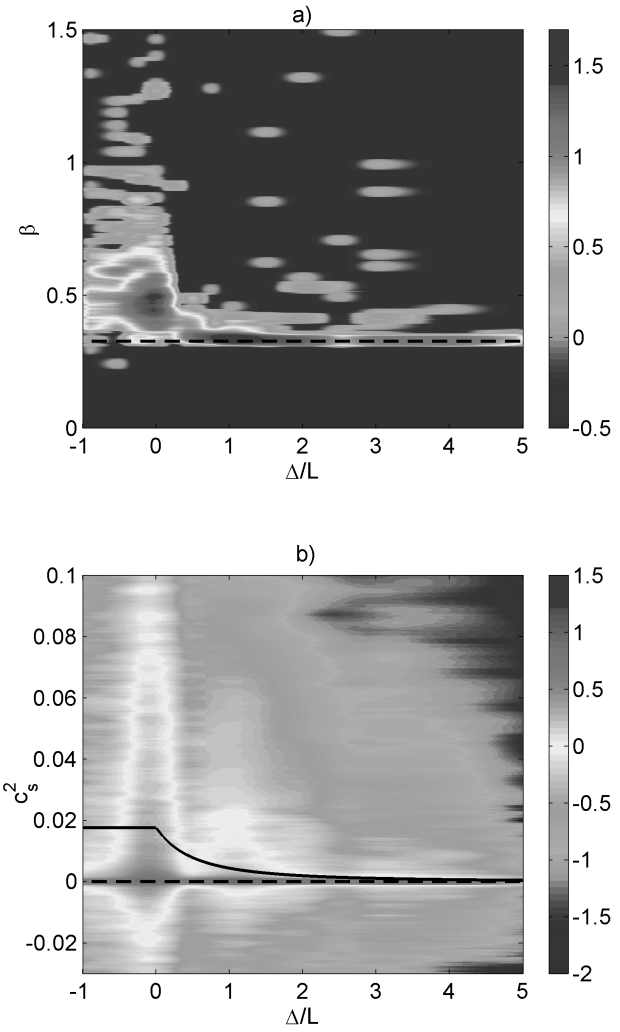

FIG. 10. Contour plots of conditional PDF of (a) β and (b) $(c_s^{(\Delta,\mathrm{sd-dyn})})^2$ from the scale-dependent dynamic model. The contours show (a) $\log_{10}P(\beta\,|\,\Delta/L)$ and (b) $\log_{10}P(c_s^2\,|\,\Delta/L)$. The averaging time to compute $c_s^{(\Delta)}$ and β is $T_c = 3.2$ s $\sim 2.0\Delta/\langle u\rangle$. The dashed line in (a) shows $\beta = 0.327$ [cf. Eq. (15)]. The dashed and solid lines in (b) show $(c_s^{\Delta})^2 = 0$ and the empirical fit of Eq. (14), respectively.

$\langle |\bar{\tilde{S}}|\bar{\tilde{S}}_{ij}L_{ij}\rangle$ or $\langle |\hat{\tilde{S}}|^2\hat{\tilde{S}}_{ij}\hat{\tilde{S}}_{ij}\rangle$ are evaluated over a time scale T_c. Figure 9 shows a few representative polynomials $P(\beta)$ for the case $T_c = 6.8$ min for three values of Δ/L. The largest root is the value of β that solves the condition of Eqs. (A1) and (A2) (POR).

Parameter β is computed for the short-duration averaging time of $T_c = 3.2$, and β is obtained in each segment. The conditional PDF of β is presented in Fig. 10a, where the β range ($0 < \beta < 1.5$) is divided into 150 bins. Note that β also depends on stability. In very stable conditions most β values are close to 0.3. The lower bound of β can be explained by considering the limit of $c_s^{(\Delta)}$ for small L: $c_s^{(\Delta)} \propto (\Delta/L)^{-1}$. Consequently,

$$\beta = \frac{(c_s^{(1.75\Delta)})^2}{(c_s^{(\Delta)})^2} \to \frac{(1/1.75\Delta)^2}{(1/\Delta)^2} = \left(\frac{1}{1.75}\right)^2 \approx 0.327. \quad (15)$$

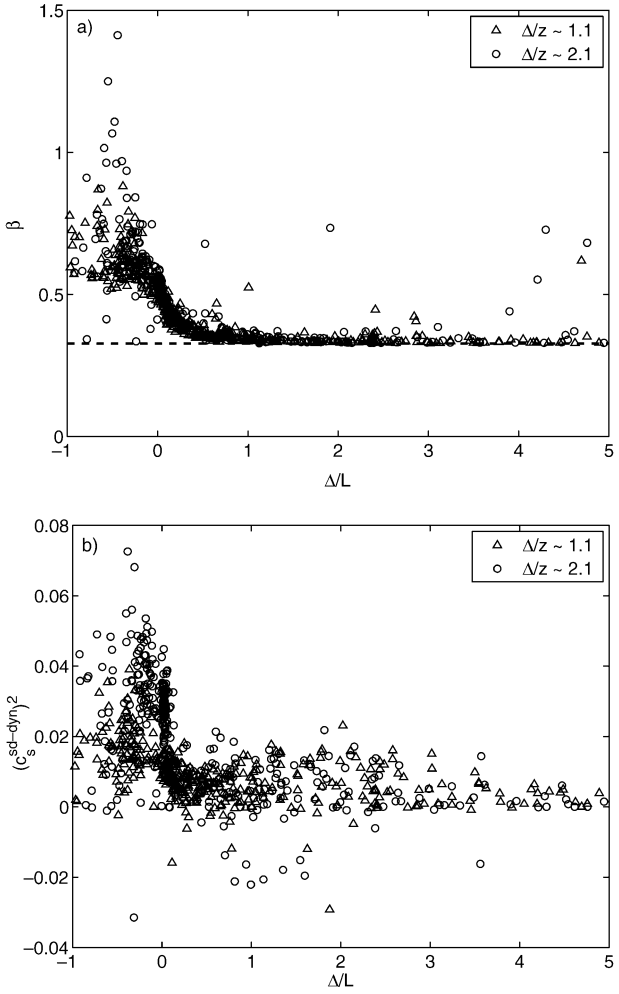

FIG. 11. Arrays 1 and 2 (a) β and (b) $c_s^{(\Delta,\text{sd–dyn})}$ as a function of Δ/L. The averaging time is $T_c = 6.8$ min.

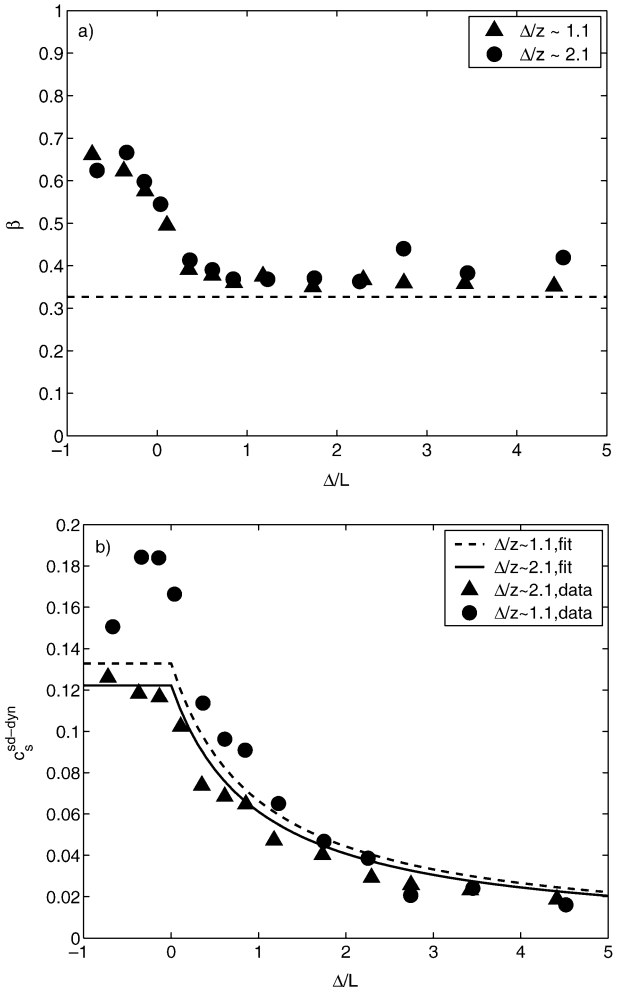

FIG. 12. (a) Scale-dependence parameter β for array 1 ($\Delta/z \sim 2.1$) and array 2 ($\Delta/z \sim 1.1$). (b) Comparison of $c_s^{(\Delta,\text{sd–dyn})}$ (symbols) with empirical fits for $c_s^{(\Delta,\text{emp})}$ of Kleissl et al. (2003) [Eq. (14)]. Variables are averaged over all segments in each stability bin.

For $\Delta/L < 0.5$, β increases and reaches a most likely value of $\beta \sim 0.5$. Recall that for scale invariance one would expect a limiting behavior of $\beta \sim 1$. Here we obtain $\beta < 1$ since even in the neutral case $\Delta > z$ and thus $\beta < 1$ for the reasons explored in POR. The data analysis is repeated by increasing the averaging time T_c to cover segments of length $T_c = 6.8$ min, as well as over very long averaging covering all data segments in each stability bin. Results are shown in Figs. 11a and 12a, respectively. The observations from results for $T_c = 3.2$ s (Fig. 10a) are confirmed since β is close to its lower bound 0.327 for $\Delta/L > 1$ and increases to values between 0.5 and 0.7 in neutral and unstable conditions. The parameter β is very similar for $\Delta/z \sim 2.1$ and for $\Delta/z \sim 1.1$. The magnitude of β in the present analysis compares well with Fig. 10 in POR. They obtain a significant increase from $\beta \sim 0.5$ at $\Delta/z = 2$ to $\beta \sim 0.65$ at $\Delta/z = 1.1$ in neutral conditions ($\Delta/L = 0$), quite consistent with present field measurement results. The limit of large z/Δ ($\Delta \ll z$), where the turbulence is better resolved, cannot be verified with the HATS data for which Δ is comparable or larger than z. Figure 13 shows that the median of β is constant with averaging time and the variability decreases with T_c.

The model coefficient, $c_s^{(\Delta,\text{sd–dyn})}$, predicted from the scale-dependent dynamic model, is obtained by replacing the measured β value in the expression for N_{ij} (see section 2d). The analysis is performed again using several averaging times $T_c = 3.2$ s, $T_c = 6.8$ min, as well as a large T_c encompassing all available data in each bin. As before, results for $T_c = 3.2$ s are presented in terms of a conditional PDF for $c_s^{(\Delta,\text{sd–dyn})}$ for the case $\Delta/z \sim 1.1$ and $-1 < \Delta/L < 5$ in Fig. 10b. The general trend in the relationship with stability is similar to that observed for $c_s^{(\Delta,\text{dyn})}$ in Fig. 5, but the spread in the PDF is considerably larger. Results from the intermediate time scale $T_c = 6.8$ min, in which β computed at that time scale is used, are shown in Fig. 11b. Results clearly show that the scale-dependent dynamic model predicts $c_s^{(\Delta,\text{emp})}$ quite well in unstable and neutral conditions. In

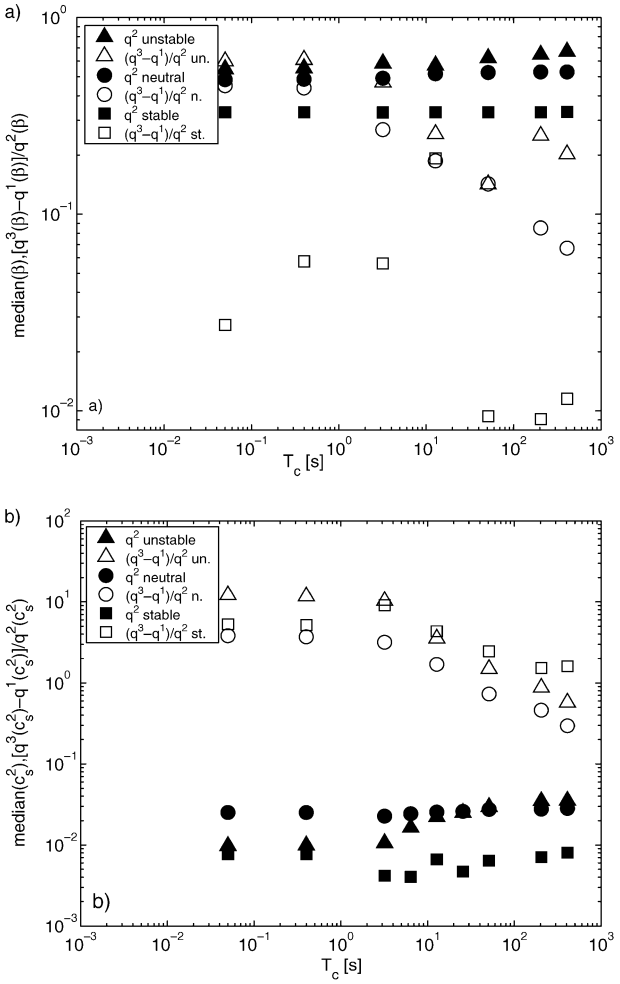

FIG. 13. Median q^2 and spread $(q^3 - q^1)/q^2$ of the (a) β and (b) $(c_s^{\Delta,\mathrm{sd-dyn}})^2$ distributions as a function of averaging time scale T_c for different stabilities: unstable ($-0.5 < \Delta/L < -0.25$), near neutral ($0 < \Delta/L < 0.25$), and stable ($2 < \Delta/L < 2.5$). The data are from array 2.

stable conditions, the prediction is still improved compared to the dynamic model (Fig. 6), but significant scatter persists. Finally, we present results using the longest T_c, by averaging over the entire dataset in each stability bin. Results are shown in Fig. 12b. As can be seen $c_s^{(\Delta,\mathrm{sd-dyn})}$ obtained from long time averaging predicts $c_s^{(\Delta,\mathrm{emp})}$ and its dependence on stability and height quite accurately.

The variability of $c_s^{(\Delta,\mathrm{sd-dyn})}$ is examined in Fig. 13b. The variability is larger than for $c_s^{(\Delta,\mathrm{emp})}$ and it reduces subsequently for $T_c > 3.2$ s. Also, in unstable conditions the median increases significantly with averaging time for $T_c > 3.2$ s. If a reasonable criterion is introduced that requires the median of $c_s^{(\Delta,\mathrm{sd-dyn})}$ to differ less than 10% from the median of $c_s^{(\Delta,\mathrm{emp})}$, then Fig. 13b suggests that the Eulerian averaging time scale T_c should correspond to at least 12.8 s, or about eight filter scales ($8 \approx 12.8\langle u\rangle/\Delta$).

To confirm that we have obtained results that are unique to turbulence signals under the present physical conditions and do not occur for any time series of random numbers, the procedure to compute dynamic and scale-dependent dynamic coefficients is tested with a time series of random velocity vectors. We generate random velocity fluctuations by distributing 3D vectors whose length is sampled from a uniform distribution in [0, 1] m s^{-1}, and whose direction is uniformly distributed over a sphere. Both white-noise and colored-noise signals (with a $-5/3$ energy spectrum for each velocity component) are used. The resulting $c_s^{(\Delta,\mathrm{emp})}$, $c_s^{(\Delta,\mathrm{dyn})}$, and $c_s^{(\Delta,\mathrm{sd-dyn})}$ feature symmetric PDFs with a strong peak at $(c_s^{(\Delta)})^2 = 0$, that is, as expected random signals do not have the correlations between L_{ij} and M_{ij} associated with net energy flux to smaller scales and a nonzero value of the coefficient. The resulting PDF for β is positively skewed, increasing for $\beta > 0.327$ and but reaching a peak at $\beta \sim 0.45$. This is significantly different from the results of the present paper, where for example the peak in $P(\beta|\Delta/L)$ for stable conditions in Fig. 10a is narrow and much closer to 0.327.

4. Conclusions

Predictions of the scale-invariant dynamic SGS model (Germano et al. 1991) and the scale-dependent dynamic SGS model (Porté-Agel et al. 2000a) for the Smagorinsky coefficient $c_s^{(\Delta)}$ have been tested a priori with a large dataset from two horizontal arrays of fourteen 3D sonic anemometers in the atmospheric surface layer. Figures 14a and 14b summarize the results by comparing the empirically determined $c_s^{(\Delta,\mathrm{emp})}$ with predictions from scale-invariant and scale-dependent dynamic models for both values of Δ/z considered. Clearly, the scale-invariance assumption of the dynamic model breaks down when the filter size is large ($\Delta > z$ or $\Delta > L$), resulting in coefficients that are too small. In an LES of the ABL this is expected to lead to unrealistic velocity profiles near the surface and a pileup of energy reflected in flat velocity spectra.

The scale-dependent dynamic model accounts for scale dependence of the coefficient. As a result the predicted coefficient is close to the value measured by the dissipation balance. It needs to be stressed that the additional parameter introduced by the scale-dependent dynamic model β is not empirically tuned, but rather determined dynamically from the large scales. Despite the resulting improvement in predicting the coefficient that produces the correct SGS dissipation compared to the scale-invariant dynamic model, it is reiterated that even ''perfect'' prediction of the coefficient does not increase the correlation between measured and modeled SGS stresses. This deficiency of the eddy-viscosity closure is related to misalignment of the eigenvectors of SGS stress and strain-rate tensors.

The results for the scale-dependent dynamic model show that short time averaging yields predicted coefficients that fluctuate greatly. This can be problematic

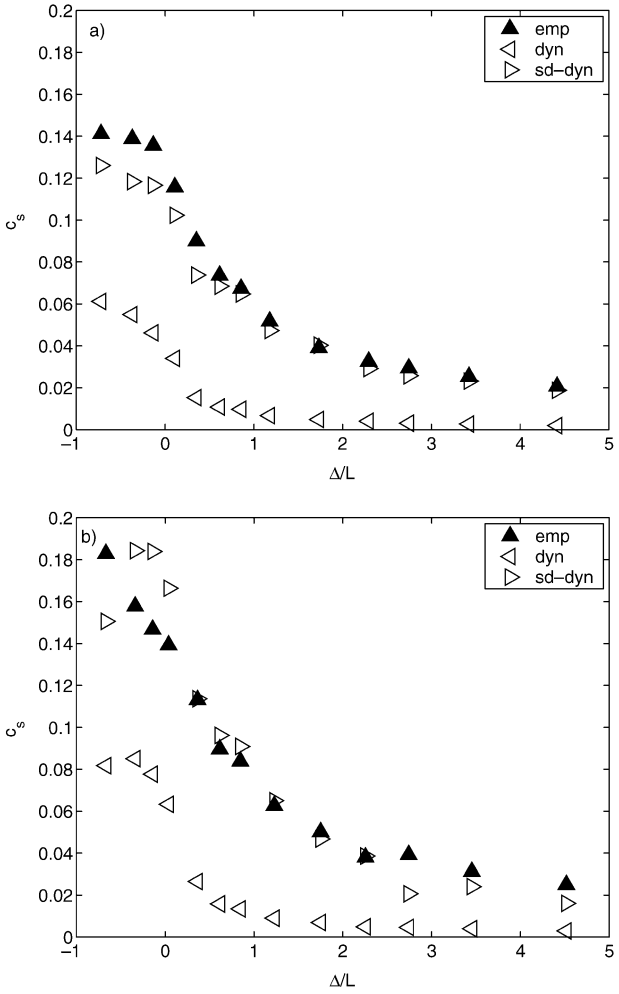

FIG. 14. Smagorinsky coefficient $c_s^{(\Delta)}$ as a function of Δ/L for different SGS models. Variables are averaged over all segments in each stability bin. (a) Array 1, $\Delta/z \sim 2.1$ and (b) array 2, $\Delta/z \sim 1.1$.

in implementations where the extent of averaging is limited (e.g., flows in complex geometries). The data also suggest that the scatter in the prediction is reduced when the Eulerian averaging time scale is greater than ~8 times the time scale associated with the filter scale. Such a time scale is somewhat larger than averaging time scales usually employed in the Lagrangian dynamic model (Meneveau et al. 1996). However, due to the fundamental differences between Lagrangian and Eulerian averaging the applicability of the result to Lagrangian averaging is uncertain and remains to be explored in simulations.

Acknowledgments. HATS measurements were made by the NCAR Integrated Surface Flux Facility. The authors wish to thank Tom Horst, Donald Lenschow, Chin-Hoh Moeng, Peter Sullivan, and Jeffrey Weil from the NCAR-ATD and MMM divisions for the fruitful collaboration during the field experiment. Thanks also to Profs. W. Eichinger, F. Porté-Agel, S. Richardson, and J. Wyngaard for the loan of sonic anemometers. We thank the anonymous reviewers of this paper for their constructive feedback. The authors gratefully acknowledge funding from the National Science Foundation, Grant NSF-ATM 0130766.

APPENDIX

Evaluation of β

From the introduction it is known that $(c_s^{(\Delta)})^2 = \langle L_{ij}M_{ij}\rangle/\langle M_{ij}M_{ij}\rangle = \langle Q_{ij}N_{ij}\rangle/\langle N_{ij}N_{ij}\rangle$. This equality can be rewritten as

$$\langle L_{ij}M_{ij}\rangle\langle N_{ij}N_{ij}\rangle - \langle Q_{ij}N_{ij}\rangle\langle M_{ij}M_{ij}\rangle = 0, \quad \text{(A1)}$$

which has two unknowns, $\beta = (c_s^{(\alpha\Delta)})^2/(c_s^{(\Delta)})^2$ and $\theta = (c_s^{(\alpha^2\Delta)})^2/(c_s^{(\Delta)})^2$. As shown in POR, one unknown can be eliminated by assuming a basic functional form of the scale dependence of the coefficient. A power-law assumption $(c_s^{(\alpha\Delta)})^2 = (c_s^{(\Delta)})^2\alpha^\phi$ yields $\theta = \beta^2$. After substituting, Eq. (A1) can be written as a fifth-order polynomial in β:

$$P(\beta) \equiv A_0 + A_1\beta + A_2\beta^2 + A_3\beta^3 + A_4\beta^4 + A_5\beta^5 = 0. \quad \text{(A2)}$$

Above,

$$A_0 = b_2c_1 - b_1c_2, \qquad A_1 = a_1c_2 - b_2e_1, \quad \text{(A3)}$$

$$A_2 = b_2d_1 + b_1e_2 - a_2c_1, \qquad A_3 = a_2e_1 - a_1e_2, \quad \text{(A4)}$$

$$A_4 = -a_2d_1 - b_1d_2, \qquad A_5 = a_1d_2, \quad \text{(A5)}$$

where

$$a_1 = -2\alpha^2\Delta^2\langle|\bar{\tilde{S}}|\bar{\tilde{S}}_{ij}L_{ij}\rangle, \qquad a_2 = -2\alpha^4\Delta^2\langle|\hat{\bar{\tilde{S}}}|\hat{\bar{\tilde{S}}}_{ij}Q_{ij}\rangle, \quad \text{(A6)}$$

$$b_1 = -2\Delta^2\langle\overline{|\tilde{S}|\tilde{S}_{ij}}L_{ij}\rangle, \qquad b_2 = -2\Delta^2\langle\widehat{|\tilde{S}|\tilde{S}_{ij}}Q_{ij}\rangle, \quad \text{(A7)}$$

$$c_1 = 4\Delta^4\langle\overline{|\tilde{S}|\tilde{S}_{ij}}\,\overline{|\tilde{S}|\tilde{S}_{ij}}\rangle, \qquad c_2 = 4\Delta^4\langle\widehat{|\tilde{S}|\tilde{S}_{ij}}\,\widehat{|\tilde{S}|\tilde{S}_{ij}}\rangle, \quad \text{(A8)}$$

$$d_1 = 4\alpha^4\Delta^4\langle|\bar{\tilde{S}}|^2\bar{\tilde{S}}_{ij}\bar{\tilde{S}}_{ij}\rangle, \qquad d_2 = 4\alpha^8\Delta^4\langle|\hat{\bar{\tilde{S}}}|^2\hat{\bar{\tilde{S}}}_{ij}\hat{\bar{\tilde{S}}}_{ij}\rangle, \quad \text{(A9)}$$

$$e_1 = 8\alpha^2\Delta^4\langle|\bar{\tilde{S}}|\bar{\tilde{S}}_{ij}\overline{|\tilde{S}|\tilde{S}_{ij}}\rangle, \qquad e_2 = 8\alpha^4\Delta^4\langle|\hat{\bar{\tilde{S}}}|\hat{\bar{\tilde{S}}}_{ij}\widehat{|\tilde{S}|\tilde{S}_{ij}}\rangle. \quad \text{(A10)}$$

REFERENCES

Bardina, J., J. H. Ferziger, and W. C. Reynolds, 1980: Improved subgrid scale models for large eddy simulation. AIAA Paper 80-1357.

Bastiaans, R. J. M., C. C. M. Rindt, and A. A. van Steenhoven, 1998:

Experimental analysis of a confined transitional plume with respect to subgrid-scale modelling. *Int. J. Heat Mass Transfer,* **41,** 3989–4007.
Canuto, V. M., and Y. Cheng, 1997: Determination of the Smagorinsky–Lilly constant c_s. *Phys. Fluids,* **9,** 1368–1378.
Cerutti, S., and C. Meneveau, 2000: Statistics of filtered velocity in grid and wake turbulence. *Phys. Fluids,* **12,** 1143–1165.
Clark, R. A., J. H. Ferziger, and W. C. Reynolds, 1979: Evaluation of subgrid models using an accurately simulated turbulent flow. *J. Fluid Mech.,* **91,** 1–16.
Deardorff, J. W., 1970: A numerical study of three-dimensional turbulent channel flow at large Reynolds numbers. *J. Fluid Mech.,* **41,** 453–480.
——, 1980: Stratocumulus-capped mixed layers derived from a three dimensional model. *Bound.-Layer Meteor.,* **18,** 495–527.
Germano, M., 1992: Turbulence: The filtering approach. *J. Fluid Mech.,* **238,** 325–336.
——, U. Piomelli, P. Moin, and W. H. Cabot, 1991: A dynamic subgrid-scale eddy viscosity model. *Phys. Fluids,* **A3,** 1760–1765.
Ghosal, S., T. S. Lund, P. Moin, and K. Akselvoll, 1995: A dynamic localization model for large eddy simulation of turbulent flow. *J. Fluid Mech.,* **286,** 229–255.
Higgins, C., M. B. Parlange, and C. Meneveau, 2003: Alignment trends of velocity gradients and subgrid scale fluxes in the turbulent atmospheric boundary layer. *Bound.-Layer Meteor.,* **109,** 59–83.
Horst, T. W., J. Kleissl, D. H. Lenschow, C. Meneveau, C.-H. Moeng, M. B. Parlange, P. P. Sullivan, and J. C. Weil, 2004: HATS: Field observations to obtain spatially filtered turbulence fields from crosswind arrays of sonic anemometers in the atmospheric surface layer. *J. Atmos. Sci.,* **61,** 1566–1581.
Hunt, J. C. R., D. D. Stretch, and R. E. Britter, 1988: Length scales in stably stratified turbulent flows and their use in turbulence models. *Stably Stratified Flows and Dense Gas Dispersion,* J. S. Puttock, Ed., Clarendon Press, 285–322.
Kleissl, J., C. Meneveau, and M. B. Parlange, 2003: On the magnitude and variability of subgrid-scale eddy-diffusion coefficients in the atmospheric surface layer. *J. Atmos. Sci.,* **60,** 2372–2388.
Lesieur, M., and O. Métais, 1996: New trends in large-eddy simulations of turbulence. *Annu. Rev. Fluid Mech.,* **28,** 45–82.
Lilly, D. K., 1967: The representation of small-scale turbulence in numerical simulation experiments. *Proc. 10th Scientific Computing Symp. on Environmental Sciences,* Yorktown Heights, NY, IBM, 195–210.
——, 1992: A proposed modification of the Germano subgrid-scale closure method. *Phys. Fluids,* **A4,** 633–635.
Liu, S., C. Meneveau, and J. Katz, 1994: On the properties of similarity subgrid-scale models as deduced from measurements in a turbulent jet. *J. Fluid Mech.,* **275,** 83–119.
——, ——, and ——, 1995: Experimental study of similarity subgrid-scale models of turbulence in the far-field of a jet. *Appl. Sci. Res.,* **54,** 177–190.
Mason, P. J., 1994: Large-eddy simulation: A critical review of the technique. *Quart. J. Roy. Meteor. Soc.,* **120,** 1–26.
McMillan, O. J., and J. H. Ferziger, 1979: Direct testing of subgrid-scale models. *AIAA J.,* **17,** 1340.
Meneveau, C., 1994: Statistics of turbulence subgrid-scale stresses: Necessary conditions and experimental tests. *Phys. Fluids,* **A6,** 815–833.
——, and J. Katz, 2000: Scale-invariance and turbulence models for large-eddy simulation. *Annu. Rev. Fluid Mech.,* **32,** 1–32.
——, T. Lund, and W. Cabot, 1996: A Lagrangian dynamic subgrid-scale model of turbulence. *J. Fluid Mech.,* **319,** 353–385.
Moeng, C.-H., 1984: A large-eddy simulation model for the study of planetary boundary-layer turbulence. *J. Atmos. Sci.,* **41,** 2052–2062.
Najjar, F. M., and D. K. Tafti, 1996: Study of discrete test filters and finite difference approximations for the dynamic subgrid-scale stress model. *Phys. Fluids,* **8,** 1076–1088.
Piomelli, U., 1999: Large-eddy simulation: Achievements and challenges. *Prog. Aerosp. Sci.,* **35,** 335–362.
Pope, S. B., 2000: *Turbulent Flows.* Cambridge University Press, 771 pp.
Porté-Agel, F., C. Meneveau, and M. B. Parlange, 1998: Some basic properties of the surrogate subgrid-scale heat flux in the atmospheric boundary layer. *Bound.-Layer Meteor.,* **88,** 425–444.
——, ——, and ——, 2000a: A scale-dependent dynamic model for large-eddy simulation: Application to a neutral atmospheric boundary layer. *J. Fluid Mech.,* **415,** 261–284.
——, M. B. Parlange, C. Meneveau, W. Eichinger, and M. Pahlow, 2000b: Subgrid-scale dissipation in the atmospheric surface layer: Effects of stability and filter dimension. *J. Hydrometeor.,* **1,** 75–87.
——, M. Pahlow, C. Meneveau, and M. B. Parlange, 2001a: Atmospheric stability effect on subgrid-scale physics of large-eddy simulation. *Adv. Water Resour.,* **24,** 1085–1102.
——, M. B. Parlange, C. Meneveau, and W. E. Eichinger, 2001b: A priori field study of the subgrid-scale heat fluxes and dissipation in the atmospheric surface layer. *J. Atmos. Sci.,* **58,** 2673–2698.
Redelsperger, J., F. Mahe, and P. Carlotti, 2001: A simple and general subgrid model suitable both for surface layer and free stream turbulence. *Bound.-Layer Meteor.,* **101,** 375–408.
Smagorinsky, J., 1963: General circulation experiments with the primitive equations. I. The basic experiment. *Mon. Wea. Rev.,* **91,** 99–164.
Sullivan, P. P., T. W. Horst, D. H. Lenschow, C.-H. Moeng, and J. C. Weil, 2003: Structure of subfilter-scale fluxes in the atmospheric surface layer with application to large eddy simulation modeling. *J. Fluid Mech.,* **482,** 101–139.
Tong, C., J. C. Wyngaard, S. Khanna, and J. G. Brasseur, 1998: Resolvable- and subgrid-scale measurement in the atmospheric surface layer: Technique and issues. *J. Atmos. Sci.,* **55,** 3114–3126.
——, ——, and J. G. Brasseur, 1999: Experimental study of the subgrid-scale stresses in the atmospheric surface layer. *J. Atmos. Sci.,* **56,** 2277–2292.
Vasilyev, O. V., T. S. Lund, and P. Moin, 1998: A general class of commutative filters for LES in complex geometries. *J. Comput. Phys.,* **146,** 82–104.